

Efficient Electromagnetic Analysis of a Dispersive Head Model Due to Smart Glasses Embedded Antennas at Wi-Fi and 5G Frequencies

Fatih Kaburcuk¹ and Atef Z. Elsherbeni²

¹Department of Electrical-Electronics Engineering
Sivas Cumhuriyet University, Sivas 58140, Turkey
fkaburcuk@cumhuriyet.edu.tr – fkaburcu@syr.edu

²Department of Electrical Engineering
Colorado School of Mines, Golden, CO 80401, United States
aelsherb@mines.edu

Abstract — Numerical study of electromagnetic interaction between an adjacent antenna and a human head model requires long computation time and large computer memory. In this paper, two speeding up techniques for a dispersive algorithm based on finite-difference time-domain method are used to reduce the required computation time and computer memory. In order to evaluate the validity of these two speeding up techniques, specific absorption rate (SAR) and temperature rise distributions in a dispersive human head model due to radiation from an antenna integrated into a pair of smart glasses are investigated. The antenna integrated into the pair of smart glasses have wireless connectivity at 2.4 GHz and 5th generation (5G) cellular connectivity at 4.9 GHz. Two different positions for the antenna integrated into the frame are considered in this investigation. These techniques provide remarkable reduction in computation time and computer memory.

Index Terms — 5G, dispersive head, FDTD method, SAR, smart glasses, temperature rise, Wi-Fi.

I. INTRODUCTION

Due to recent increase of wireless and mobile communication capabilities with the 5th generation (5G) technology and the use of higher frequencies for smart communication devices, there is a great need to assessment of electromagnetic (EM) wave penetration and related temperature rise in the human head.

With the recent introduction of 5G technology, the use of smart wearable devices such as smart watches and smart glasses has increased in popularity. Currently, smart glasses, manufactured by different companies [1-3], utilize wireless connectivity based on Bluetooth and Wi-Fi around the 2.4 GHz band. Future smart glasses would include antennas operating for Wi-Fi and 5G cellular connectivity. It is universally recognized that the EM fields radiated from the adjacent antennas to a

human head may be harmful to human health. As a consequence, it is important to assess the effects of EM fields on the human head and report the corresponding SAR and temperature rise distributions.

The numerical calculation of EM interaction between an antenna and a three dimensional (3D) human head model has been performed in [4-9] using the finite-difference time-domain (FDTD) method. It requires long computation time and large computer memory because the number of cell in the computational domain is more than several millions, especially for high frequencies with proper resolution. This makes such calculations impossible on ordinary desktop computers. A dispersive algorithm proposed in [9] provides remarkable reduction in the computation time to analyze a dispersive head model at multiple frequencies of interest in a single simulation. However, as the frequencies get higher, this reduction is not sufficient to simulate the entire human head model with the ordinary desktop computers.

The effect of EM radiation produced by a cellular phone on a human head with regular glasses made of metallic frames was investigated using an EM commercial software [10-12] and the traditional FDTD method [13-14]. By using an EM commercial software, the effects of an antenna integrated into the pair of smart glasses for Wi-Fi connectivity [15-18] and 4G cellular connectivity [19-23] on the human head have been studied to investigate the radiation pattern and SAR distribution in the head. In the previous studies [15-23], analysis of SAR in the human head due to the smart glasses was performed at only one frequency of interest using a single simulation while ignoring the dispersive characteristics of the biological tissues of the head. The temperature rise in the head due to an integrated antenna into the pair of smart glasses has not been considered yet.

In this paper, the algorithm proposed in [9] is used to obtain radiation pattern, SAR and temperature rise distributions in the dispersive head at multiple

frequencies of interest in a single simulation. This algorithm, which will be referred to as a dispersive algorithm, is based on the Debye model of the head tissue parameters to be used in auxiliary differential equation (ADE) formulation of the FDTD method [24]. Then the calculations of SAR and temperature rise with the help of Pennes bioheat equation [25] are performed. In the Debye model, the three-term Debye coefficients calculated and tabulated in [26] are used as the dispersive EM properties of the human head tissues to obtain solutions at a wide range of frequencies (500 MHz to 20 GHz). The work presented here is an extension of the preliminary work presented in [27].

The effect of the integrated antenna into the pair of smart glasses on a realistic head model is investigated to evaluate the validity of two speeding up techniques for the dispersive algorithm. The integrated antenna is designed to operate at two frequency bands for Wi-Fi at 2.4 GHz and 5G cellular at 4.9 GHz. In order to show the effect of the position of the integrated antenna on the pair of smart glasses on the human head, the antennas integrated into the frame have been placed in two different positions closest to the eye, the most sensitive organ. The spatial-peak SAR over any 1 gram of tissue (SAR_{1g}), 10 gram of tissue (SAR_{10g}) in the head, and temperature rise distributions in the head at 2.4 and 4.9 GHz are computed for each antenna position. Numerical results show that the speeding up techniques would be efficient for analyzing the head model due to EM waves of higher frequencies.

Two speeding up techniques are used here and the electromagnetic effects of smart glasses on the human head are investigated using the dispersive algorithm with these techniques. The speeding up technique proposed in [28] for anisotropic materials is applied to the dispersive algorithm and based on dividing the computation domain into two regions: one is the dispersive region analyzed using the dispersive formulation [24] and the other is non-dispersive region analyzed using the non-dispersive formulation [24]. The other speeding up technique is to use a half head model instead of the full head model in the FDTD simulations. These speeding up techniques provides more than 50% reduction in computation time and computer memory.

II. COMPUTATION METHODS AND MODELS

A. 3D human head model with dispersive tissues

A human head model generated in [29] and used in this work consists of eight tissues (skin, muscle, bone, blood, fat, lens, and white and grey matter). Figure 1 shows a sample of a horizontal slice of the human head model which consists of 172 (width) \times 218 (depth) \times 240 (height) cubic cells.

The EM parameters of all tissues in the human body

are frequency dependent. Therefore, with a traditional FDTD solution one can obtain results due to only one frequency in a single simulation. The numerical technique proposed provides the three-term Debye coefficients tabulated in [26] for the biological tissues in the frequency range between 500 MHz and 20 GHz. The complex relative permittivity ($\epsilon_r^*(\omega)$) for the three-term Debye coefficients is defined [26] as:

$$\epsilon_r^*(\omega) = \epsilon_\infty + \sum_{k=1}^3 \frac{\Delta\epsilon_k}{1+j\omega\tau_k}; \Delta\epsilon_k = A_k(\epsilon_s - \epsilon_\infty), \quad (1)$$

where ϵ_∞ is permittivity at high frequencies, $\Delta\epsilon_k$ is pole weight, and τ_k is relaxation time.

In order to ensure the numerical stability in the FDTD method, the cell size (Δ) should be less than $\lambda_{min}/10$ [6-7] and expressed as:

$$\Delta = \frac{\lambda_{min}}{10} = \frac{c}{10f_{max}\sqrt{real(\epsilon_r^*)}}, \quad (2)$$

where λ_{min} is the wavelength of the highest frequency (f_{max}) in the head model and c is the speed of light in free space. The head model is rescaled to have a cell size of $\Delta=0.9$ mm (about $\lambda_{min}/10$ in the head model exposed to EM waves at 4.9 GHz) in all directions to ensure the numerical stability.

B. Speeding up techniques

In the dispersive algorithm, the electric and magnetic field components, and additional field terms due to Debye dispersive tissues [24] are calculated for every FDTD time-step in the entire computational domain. It has been realized that additional field terms do not need to be calculated in every cell of the computational domain. Therefore, a speeding up technique proposed similarly in [28] is used to reduce the computation time and computer memory. This technique called as domain division technique (DDT) is based on dividing the computation domain into two regions: one is called dispersive region which contains a dispersive head and the other is called non-dispersive region which contains air layer, convolution perfect matching layer (CPML) [24], and non-dispersive materials, as shown in Fig. 2. In the dispersive region, the dispersive formulation is performed to calculate the field components, whereas, in the non-dispersive region, the regular FDTD formulation in [24] is performed to update the field components.

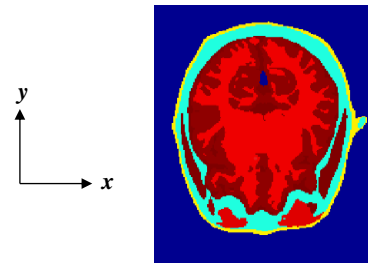


Fig. 1. Horizontal slice of the 3D realistic head model.

The penetration depth is a function of frequency and a measure of how deep the electromagnetic wave is affecting the biological tissues. In [30], the penetration depth of the electromagnetic wave for one-dimensional human head model has been extensively studied from 500 MHz to 100 GHz. According to [30] and the best of our knowledge, the penetration depth in the human head model is less than 100 mm at 500 MHz and becomes smaller as the frequency increases. It can be said that the electromagnetic waves radiated by the antenna placed on one side of the human head cannot send a significant amount of waves to the other half of the head. Therefore, it is not necessary to simulate the full head model. As the other speeding up technique, a half head model instead of full head model is used in the simulation to reduce the computation time and computer memory. In this technique, it is assumed that the cut side of half head model is terminated by 10 cell layers of CPML [24] extending to inside of the head tissues and other sides of the head model is terminated by 10 cell layers of CPML with 10 cell air layers. The number of cells for the half head model, shown in Fig. 3, cut in the x - and y -directions is 7,657,440. However, the number of cell is 15,314,880 for the entire computational domain including the full head model, 10 cell air layers and 10 cell layers of CPML. These two techniques used in this work provide more than 50% reduction in the computation time and computer memory.

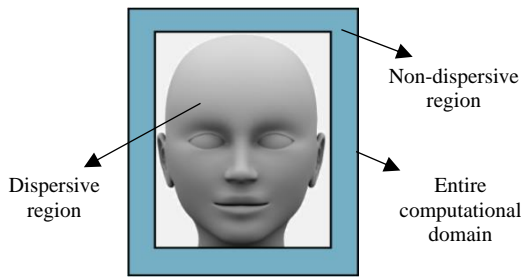


Fig. 2. Entire FDTD computational domain divided into the dispersive and non-dispersive regions.

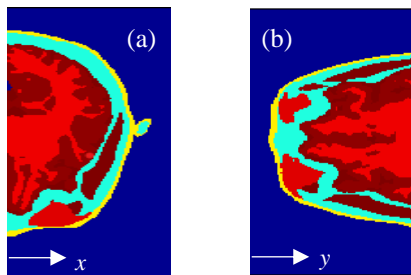


Fig. 3. Horizontal slice of the half head model cut in the (a) x - and (b) y -directions.

C. Smart glasses model and antenna

The smart glasses includes non-dispersive materials which are plastic frames, metallic hinges, lens, and antenna. The relative permittivity of lens and frame of the smart glasses is 4.82 and 3.5, respectively, and the wires of antenna are made of PEC. The configuration of the smart glasses is shown in Fig. 4 with all dimensions. In order to obtain solutions at multiple frequencies in a single simulation, the antenna integrated into the frame of the smart glasses requires to operate at least two frequency bands which will be Wi-Fi and 5G cellular connectivity for this work. The antenna, as shown in Fig. 5, consists of a dipole with two passive wires which create double resonances. The length and radius of the dipole antenna and passive wires are given in Fig. 5. Two passive wires are placed at a distance of 2.7 mm at the two sides of the dipole antenna. Two different positions for the antenna in the frame are considered: left arm of the frame and bridge of the frame as shown in Fig. 4. The combination of the dipole antenna and the two passive wires were simulated using the thin-wire formulation [24] based on the FDTD method. The input reflection coefficients (S_{11}) at the terminals of the integrated antenna placed into the frame with and without the head model are shown in Fig. 6. The resonance frequencies of the antenna have been slightly affected by the presence of the human head and a third resonance frequency appeared.

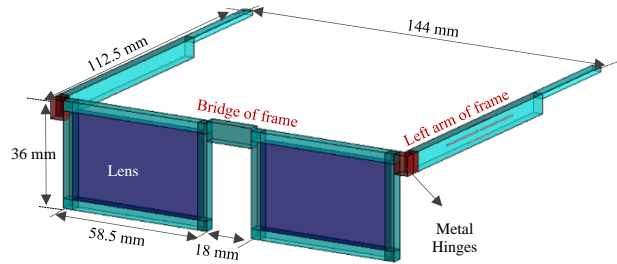


Fig. 4. Geometry of the smart glasses included lens, frame, and antenna.

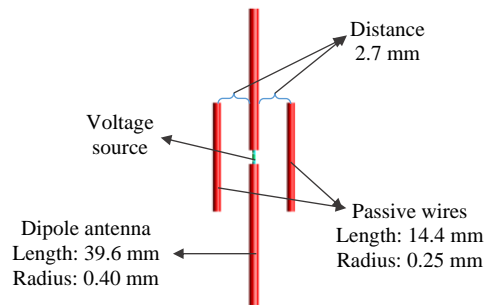


Fig. 5. Integrated dipole antenna with two passive wires.

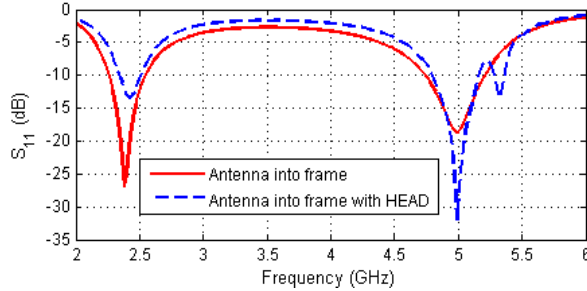


Fig. 6. S_{11} of the integrated antenna into the frame with and without the human head model.

D. SAR calculation

SAR is the ratio of absorbed RF energy per unit mass of biological tissues. The SAR values in the biological tissues are computed by using the FDTD method. The electric fields in time-domain are calculated on the edges of each cell during each FDTD time-step. The twelve-field component approach proposed in [31] is used to obtain the averaged electric field components in the center of each cell. Then, these averaged electric field components are transformed to frequency domain by using the discrete Fourier transform (DFT). After EM simulation is completed, the electric field components are obtained for the calculation of the steady-state SAR distribution in the human head model at each frequency of interest. In order to make a comparison with existing studies in [19-22], all calculated SAR values are normalized to the antenna input power of 0.25 W for each frequency of interest. For calculating SAR_{1g} and SAR_{10g} in the head model, the IEEE standard in [32] is used. The obtained SAR_{1g} values are considered as RF heat source in the temperature rise calculation.

E. Temperature rise calculation

After performing the EM simulation and SAR calculation for the head, the temperature rise calculation using the Pennes bioheat equation [25] is carried out in two parts for each frequency of interest. In the first part, the steady-state temperature distribution in the head is calculated by solving the bioheat equation with no RF heat source ($SAR_{1g}=0$). In the second part, the temperature distribution due to RF heat source is calculated by substituting the SAR_{1g} distribution into the bioheat equation. By taking the difference between the temperature distributions obtained in the two parts, the temperature rise distribution in the head is obtained. The bioheat equation computes the temperature distribution based on the tissues mass density, heat capacity, thermal conductivity, blood perfusion rate, and blood temperature. All these parameters for the tissues along with the convective boundary condition for the bioheat equation applied to the skin-air and internal cavity-air interface are presented in [4] and [9].

III. NUMERICAL RESULTS

To verify the validity of the dispersive algorithm for the smart glasses application, the SAR_{1g} values in the head using the dispersive algorithm are compared with those reported in [17] at 2.4 GHz and with those reported in [20-21] at 1.9 GHz when the antenna is placed into the left arm of the frame. The maximum SAR_{1g} value in the head at 2.4 GHz obtained using the dispersive algorithm is 0.548 W/kg, whereas that obtained in [17] using an EM commercial software is 0.557 W/kg when the input power was set to 63.095 mW. The obtained maximum SAR_{1g} value in the head at 1.9 GHz using the dispersive algorithm is 1.75 W/kg, whereas that obtained in [20-21] using an EM commercial software is 1.64 W/kg when the input power was set to 0.25 W. The compared results are in good agreement with acceptable differences. The reason for these differences in the compared results would come from the use of different head model and head resolution, and from different types of antennas used in the studies.

In order to show the performance of applying DDT and using a half head model, and the effects of the antenna positions into the frame of the smart glasses on the SAR_{1g} , SAR_{10g} , and temperature rise distributions, two different antenna positions in the frame of the glasses are evaluated at 2.4 and 4.9 GHz using the dispersive algorithm. The specification of the computer used in this work is Intel® Core™ i7-8700 CPU and 16 GB RAM. The FDTD program is developed on the 64-bit MATLAB version 8.2.0.701 (R2013a).

A. SAR and temperature rise due to the antenna integrated into the left arm of the smart glasses

The maximum SAR_{1g} , SAR_{10g} , and temperature rise values in the full head model without DDT and half head with DDT at 2.4 GHz and 4.9 GHz are obtained and tabulated in Table 1. It can be seen that applying DDT and using half head model do not affect the results. The distributions of SAR_{1g} and temperature rise obtained in the full head model without DDT and in the half head model with DDT are evaluated at 2.4 and 4.9 GHz and shown in Figs. 7 and 8, respectively. It can be realized from these figures that there are no difference in the obtained distributions and the maximum SAR_{1g} and temperature rise occur at the left side of the head because the antenna is placed into the left arm of the smart glasses. It can be also realized that the temperature rise distributions depend on the SAR distributions. In order to show the effect of the human head on the antenna radiation patterns, the radiation patterns of the antenna in the left arm of the frame with and without the human head at the resonance frequencies are calculated and shown in Fig. 9. It can be seen from the radiation patterns on the xy and xz plane cuts that the presence of the human head model greatly attenuates the radiation of the antenna

towards the head and increases in the other direction.

In Table 2, the computation time and computer memory for the EM analysis of the full human head without DDT and half human head with DDT using the dispersive algorithm are tabulated. It can be seen from Table 2 that applying DDT and using half head model in the simulations provides more than 60% reduction in computation time and 50% reduction in computer memory.

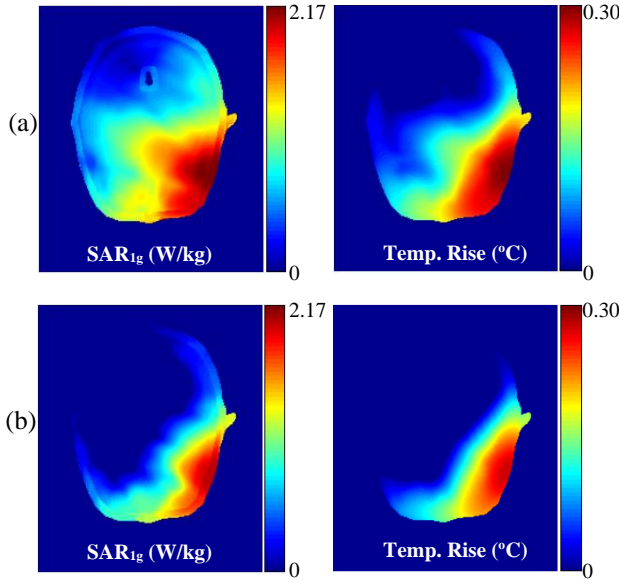


Fig. 7. SAR_{1g} and temperature rise distributions in the full head model at (a) 2.4 and (b) 4.9 GHz.

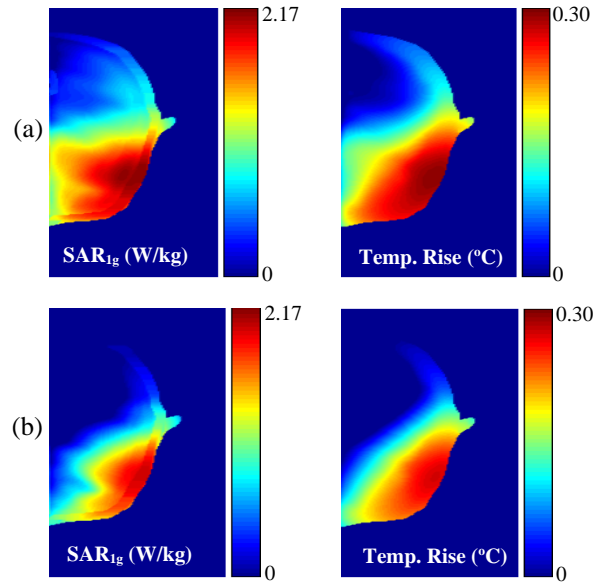


Fig. 8. SAR_{1g} and temperature rise distributions in the half head model at (a) 2.4 and (b) 4.9 GHz.

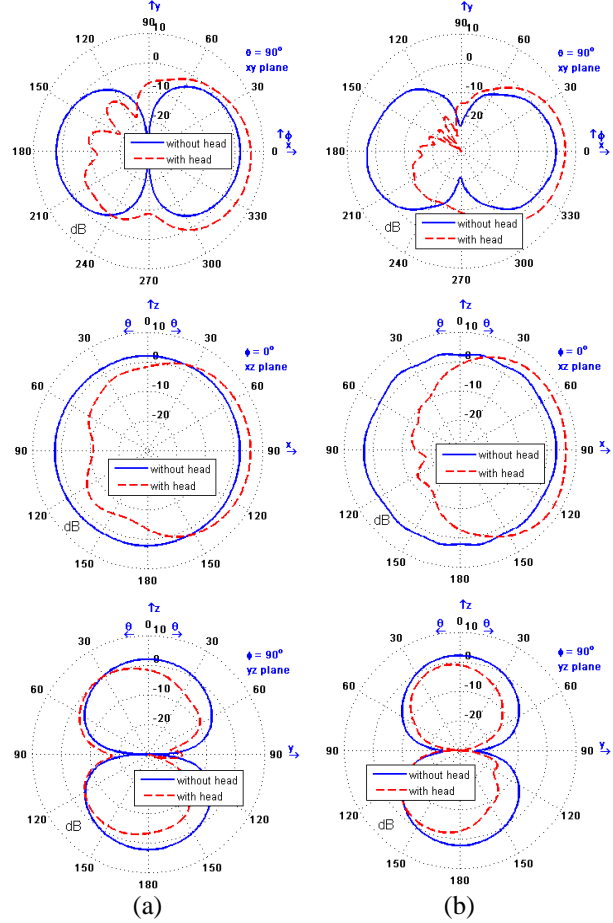


Fig. 9. Radiation patterns at (a) 2.4 and (b) 4.9 GHz with and without the head in the *xy*, *xz*, and *yz* plane cuts.

Table 1: Max. SAR and temperature rise values obtained for the full head without DDT and half head with DDT

Freq. (GHz)	Head Model	SAR _{1g} (W/kg)	SAR _{10g} (W/kg)	Max. Temp. Rise (°C)
2.4	Full Head	2.1696	1.1467	0.2990
	Half Head	2.1541	1.1409	0.2971
4.9	Full Head	1.1379	0.4676	0.1538
	Half Head	1.1375	0.4674	0.1534

Table 2: Computation time and computer memory of full and half head model

	Model	Computation Time (min.)	Computer Memory (MB)
Without DDT	Full Head	2178	8870
With DDT	Half Head	871	4380

B. SAR and temperature rise due to the antenna integrated into the bridge of the smart glasses

The maximum SAR_{1g}, SAR_{10g}, and temperature rise values in the full head model without DDT and half head with DDT at 2.4 GHz and 4.9 GHz are obtained and

tabulated in Table 3. It can be seen that applying DDT and using the half head model do not affect the results. The distributions of SAR_{1g} and temperature rise obtained in the full head model without DDT and in the half head model with DDT are evaluated at 2.4 and 4.9 GHz and shown in Figs. 10 and 11, respectively. It can be realized from these figures that there are no difference in the obtained distributions and the maximum SAR_{1g} and temperature rise occur at the front side of the head because the antenna is placed into the bridge of the smart glasses. The radiation patterns of the antenna in the bridge of the frame with and without the human head at resonance frequencies are shown in Fig. 12. It can be seen from the radiation patterns on the *xy* and *yz* plane cuts that the presence of the human head model greatly attenuates the radiation of the antenna towards the head and increases in the other direction.

In Table 4, the computation time and computer memory for the EM analysis of full human head without DDT and half human head with DDT using the dispersive algorithm are tabulated. It can be seen from Table 4 that applying DDT and using half head model in the simulations provides more than 60% reduction in computation time and 50% reduction in computer memory.

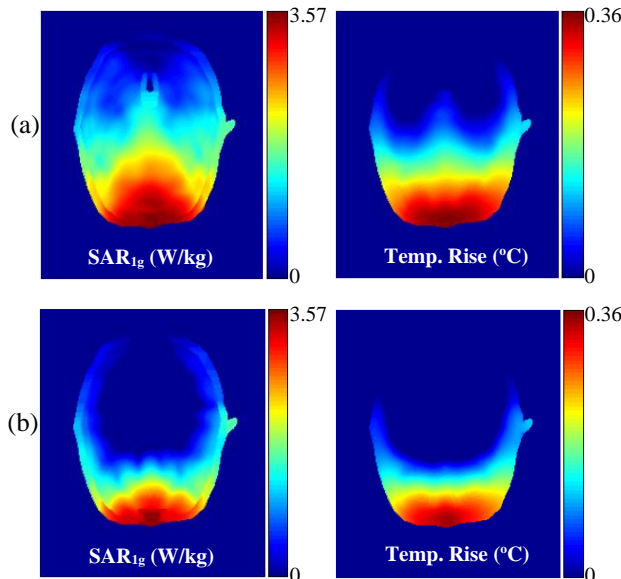


Fig. 10. SAR_{1g} and temperature rise distributions in the full head model at (a) 2.4 and (b) 4.9 GHz.

Table 3: Max. SAR and temperature rise values obtained for the full head without DDT and half head with DDT

Freq. (GHz)	Head Model	SAR _{1g} (W/kg)	SAR _{10g} (W/kg)	Max. Temp. Rise (°C)
2.4	Full Head	3.5735	1.2419	0.3606
	Half Head	3.5730	1.2415	0.3607
4.9	Full Head	2.8160	0.2670	0.2456
	Half Head	2.8171	0.2672	0.2501

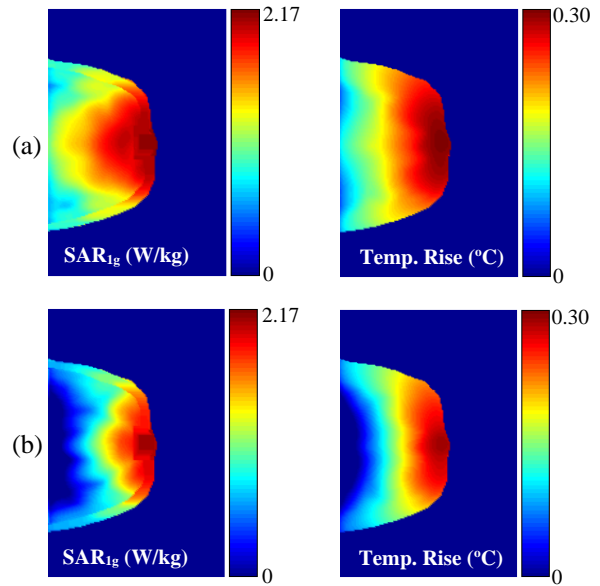


Fig. 11. SAR_{1g} and temperature rise distributions in the half head model at (a) 2.4 and (b) 4.9 GHz.

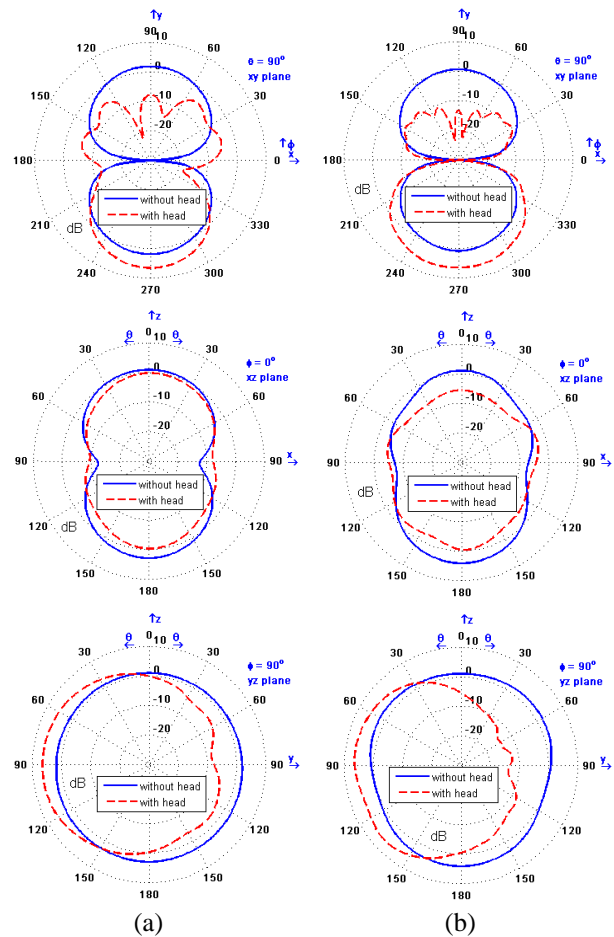


Fig. 12. Radiation patterns at (a) 2.4 and (b) 4.9 GHz with and without the head in the *xy*, *xz*, and *yz* plane cuts.

Table 4: Computation time and computer memory of full and half head model

	Model	Computation Time (min.)	Computer Memory (MB)
Without DDT	Full Head	2165	8820
With DDT	Half Head	837	4320

C. Comparison of results obtained due to the antenna into two different positions

The maximum SAR_{1g} , SAR_{10g} , and temperature rise values in the head at 2.4 GHz and 4.9 GHz are tabulated in Tables 1 and 3 when the antenna is placed into two different positions in the smart glasses. The electric conductivities of the tissues become larger as the frequency is increased, hence the magnitude of EM waves penetration in the head decreases significantly. Therefore, the SAR_{1g} , SAR_{10g} , and resulting temperature rise values in the head decrease at higher frequencies. It is well known that the SAR values are dependent on the frequency, the type of antenna, the input power of the antenna, the EM parameters of tissues, antenna polarization, the distance between the human head and the antenna, etc.

The limits of maximum SAR_{1g} and SAR_{10g} values are determined by the RF exposure guidelines and standards in [33-34]. The SAR_{1g} values reported in Tables 1 and 3 are generally above the limit of 1.6 W/kg, whereas the SAR_{10g} values reported in these tables are always less than the limit of 2 W/kg when the antenna input power is set to 0.25 W. These high values above the limit would require this power to be reduced to comply with the RF exposure guidelines and standards.

It must be noted that the distance between the antenna and human head is 13.5 mm and 7.2 mm for left arm and bridge of the frame, respectively. These distances are closer than those reported in [4-9]. The SAR and resulting temperature rise values obtained due to the antenna in the bridge of the frame are higher than those obtained due to the antenna in the left arm of the frame because the integrated antenna in the bridge of the frame is closer to the head and eye which is one of the most sensitive organs in the human head for EM field exposure.

The maximum temperature rises reported in Tables 1 and 3 are less than the temperature rise limit of 4.5 °C [35] for tissue health injury, but they are not negligible. The maximum temperature variations at 2.4 and 4.9 GHz due to the antenna placed into two different positions in the glasses frame as a function of time are shown in Fig. 13. It can be seen that the maximum temperature rises increases exponentially over the first 6 minutes, then they slow down, and the maximum temperature rises are reached after 30 minutes of exposure.

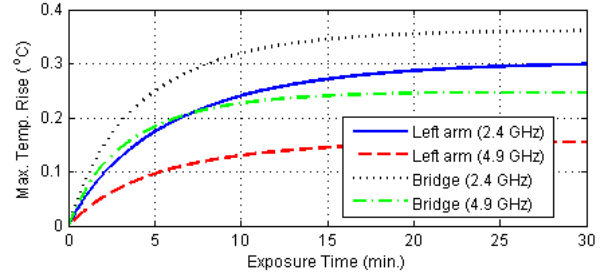


Fig. 13. Maximum temperature rise at 2.4 and 4.9 GHz due to the antenna placed into position-1 and position-2.

VI. CONCLUSION

The electromagnetic interactions between a 3D dispersive human head model and electromagnetic fields radiated by an antenna integrated into a pair of smart glasses at 2.4 and 4.9 GHz are investigated using a dispersive FDTD algorithm. Additionally, in order to show the effect of the position of the integrated antenna on the SAR and temperature rise distributions in the head, two possible positions for the antenna into the frame of the smart glasses are considered. In order to reduce to computation time and computer memory of the simulations, two speeding up techniques used in this work are based on dividing the computational domain into two sub-regions and using a half head model instead of a full head model. Applying these techniques provides more than 50% in the computation time and computer memory. These techniques would be efficient for analyzing the human head due to electromagnetic waves of higher frequencies.

REFERENCES

- [1] <https://www.vuzix.com/Products/m100-smart-glasses> [Online website 2021].
- [2] <https://x.company/glass/> [Online website 2021].
- [3] <https://www.theverge.com/2015/4/16/8422111/rec-on-jet-smart-glasses-sports-google-glass> [Online website 2021].
- [4] J. Wang and O. Fujiwara, "FDTD computation of temperature rise in the human head for portable telephones," in *IEEE Transactions on Microwave Theory and Techniques*, vol. 47, no. 8, pp. 1528-1534, Aug. 1999.
- [5] P. Bernardi, M. Cavagnaro, S. Pisa, and E. Piuzzi, "Power absorption and temperature elevations induced in the human head by a dual-band monopole-helix antenna phone," in *IEEE Transactions on Microwave Theory and Techniques*, vol. 49, no. 12, pp. 2539-2546, Dec. 2001.
- [6] A. Hirata and T. Shiozawa, "Correlation of maximum temperature increase and peak SAR in

- the human head due to handset antennas,” in *IEEE Transactions on Microwave Theory and Techniques*, vol. 51, no. 7, pp. 1834-1841, July 2003.
- [7] A. Hirata, M. Morita, and T. Shiozawa, “Temperature increase in the human head due to a dipole antenna at microwave frequencies,” in *IEEE Transactions on Electromagnetic Compatibility*, vol. 45, no. 1, pp. 109-116, Feb. 2003.
- [8] M. Fujimoto, A. Hirata, J. Q. Wang, O. Fujiwara, and T. Shiozawa, “FDTD-derived correlation of maximum temperature increase and peak SAR in child and adult head models due to dipole antenna,” in *IEEE Transactions on Electromagnetic Compatibility*, vol. 48, no. 1, pp. 240-247, Feb. 2006.
- [9] F. Kaburcuk and A. Z. Elsherbeni, “Temperature rise and SAR distribution at wide range of frequencies in a human head due to an antenna radiation,” *Applied Computational Electromagnetics Society Journal*, vol. 33, no. 4, pp. 367-372, Apr. 2018.
- [10] M. Zhang and X. Wang, “Influence on SAR due to metallic frame of glasses based on high-resolution Chinese electromagnetic human model,” *Asia-Pacific International Symposium on Electromagnetic Compatibility*, Beijing, pp. 48-51, 2010.
- [11] M. H. Mat, M. F. B. A. Malek, W. G. Whittow, S. H. Ronald, M. S. Zulkefli, N. Saudin, and L. Mohamed, “The influence of human head model wearing metal-frame spectacles to the changes of SAR and antenna gain: Simulation of frontal face exposure,” *Progress In Electromagnetics Research*, vol. 137, pp. 453-473, 2013.
- [12] G. Bellanca, G. Caniato, A. Giovannelli, P. Olivo, and S. Trillo, “Effect of field enhancement due to the coupling between a cellular phone and metallic eyeglasses,” *Microw. Opt. Technol. Lett.*, vol. 48, no. 1, pp. 63-65, Jan. 2006.
- [13] K. Stergiou, C. Panagamuwa, W. Whittow, and R. Edwards, “Effects of metallic semi-rimmed spectacles on SAR in the head from a 900MHz frontal dipole source,” *Loughborough Antennas & Propagation Conference*, Loughborough, pp. 721-724, 2009.
- [14] J. Q. Lan and K. M. Huang, “Evaluation of SAR in a human head with glasses exposed to radiation of a mobile phone,” *Journal of Electromagnetic Waves and Applications*, vol. 27, no. 15, pp. 1919-1930, 2013.
- [15] M. Ferreira, C. Oliveira, F. Cardoso, and L. M. Correia, “SAR assessment of google glasses at cellular wireless frequency bands,” *10th European Conference on Antennas and Propagation (EuCAP)*, Davos, pp. 1-4, 2016.
- [16] Y. F. Zheng, G. H. Sun, Q. K. Huang, S. W. Wong, and L. S. Zheng, “Wearable PIFA antenna for smart glasses application,” *IEEE International Conference on Computational Electromagnetics*, Guangzhou, pp. 370-372, 2016.
- [17] S. Choi and J. Choi, “Miniaturized MIMO antenna with a high isolation for smart glasses,” *IEEE-APS Topical Conference on Antennas and Propagation in Wireless Communications*, Verona, pp. 61-63, 2017.
- [18] Y. A. A. Pizarro, A. A. de Salles, S. Severo, J. L. T. Garzon, and S. M. R. Bueno, “Specific absorption rate (SAR) in the head of Google glasses and Bluetooth user’s,” *IEEE Latin-America Conference on Communications*, Cartagena de Indias, pp. 1-6, 2014.
- [19] A. Cihangir, C. Luxey, G. Jacquemod, R. Pilard, F. Giancesello, W. G. Whittow, and C. J. Panagamuwa, “Investigation of the effect of metallic frames on 4G eyewear antennas,” *Loughborough Antennas and Propagation Conference*, Loughborough, pp. 60-63, 2014.
- [20] A. Cihangir, W. G. Whittow, C. J. Panagamuwa, F. Ferrero, G. Jacquemod, F. Giancesello, and C. Luxey, “Feasibility study of 4G cellular antennas for eyewear communicating devices,” in *IEEE Antennas and Wireless Propagation Letters*, vol. 12, pp. 1704-1707, Oct. 2013.
- [21] A. Cihangir, W. Whittow, C. Panagamuwa, G. Jacquemod, F. Giancesello, and C. Luxey, “4G antennas for wireless eyewear devices and related SAR,” *Comptes Rendus Physique*, vol. 16, no. 9, pp. 836-850, Nov. 2015.
- [22] A. Cihangir, C. J. Panagamuwa, W. G. Whittow, F. Giancesello, and C. Luxey, “Ultrabroadband antenna with robustness to body detuning for 4G eyewear devices,” in *IEEE Antennas and Wireless Propagation Letters*, vol. 16, pp. 1225-1228, Nov. 2017.
- [23] J. Lan and G. Du, “Evaluation of remperature elevation in human ocular tissues due to wireless eyewear devices,” *Applied Computational Electromagnetics Society Journal*, vol. 34, no. 1, pp. 17-24, Jan. 2019.
- [24] A. Z. Elsherbeni and V. Demir, *The Finite-Difference Time-Domain Method for Electromagnetics with MATLAB Simulations*, second edition, ACES Series on Computational Electromagnetics and Engineering, SciTech Publishing, an Imprint of IET, Edison, NJ, 2016.
- [25] H. H. Pennes, “Analysis of tissue and arterial blood temperature in resting forearm,” *J. Appl. Physiol.*, vol. 1, pp. 93-122, 1948.
- [26] M. A. Eleiwa and A. Z. Elsherbeni, “Debye constants for biological tissues from 30 Hz to 20 GHz,” *Applied Computational Electromagnetics Society Journal*, vol. 16, no. 3, pp. 202-213, Nov. 2001.

- [27] F. Kaburcuk and A. Z. Elsherbeni, "Smart glasses radiation effects on a human head model at Wi-Fi and 5G cellular frequencies," *2018 International Applied Computational Electromagnetics Society Symposium - China (ACES)*, Beijing, China, pp. 1-2, 2018.
- [28] F. Kaburcuk and A. Z. Elsherbeni, "A speeding up technique for lossy anisotropic algorithm in FDTD method," *Applied Computational Electromagnetics Society Journal*, vol. 31, no. 12, pp. 1377-1381, 2016.
- [29] I. G. Zubal, C. R. Harrell, E. O. Smith, Z. Rattner, G. R. Gindi, and P. B. Hoffer, "Computerized three-dimensional segmented human anatomy," *Medical Physics*, vol. 21, no. 2, pp. 299-302, Feb. 1994.
- [30] F. Kaburcuk, A. Z. Elsherbeni, R. Lumnitzer, and A. Tanner, "Electromagnetic waves interaction with a human head model for frequencies up to 100 GHz," *Applied Computational Electromagnetics Society Journal*, vol. 35, no. 6, pp. 613-621, 2020.
- [31] K. Caputa, M. Okoniewski, and M. A. Stuchly, "An algorithm for computations of the power deposition in human tissue," in *IEEE Antennas and Propagation Magazine*, vol. 41, no. 4, pp. 102-107, Aug. 1999.
- [32] IEEE Recommended Practice for Measurements and Computations of Radio Frequency Electromagnetic Fields with Respect to Human Exposure to Such Fields, 100 kHz-300 GHz, IEEE Standard C95.3-2002, Annex E, 2002.
- [33] Federal Communications Commission, "Evaluating compliance with FCC guidelines for human exposure to radio frequency electromagnetic fields," Rep., Washington, DC, Tech. Rep. OET Bull. 65, 1997.
- [34] IEEE Standard for Safety Levels with Respect to Human Exposure to Radio Frequency Electromagnetic Fields, 3 kHz to 300 GHz, IEEE Standard C95.1, 1999.
- [35] A. C. Guyton and J. E. Hall, *Textbook of Medical Physiology*. Philadelphia, PA: W. B. Saunders, chap. 73, 1996.



Fatih Kaburcuk received both the M.Sc. and Ph.D. degrees from Syracuse University, Syracuse, NY, USA, in 2011 and 2014, respectively, all in Electrical eEngineering. During his graduate studies, he worked as a Research Assistant with Syracuse University and PPC-Belden Inc. in Liverpool, NY, USA. He worked as a Visiting Research

Scholar at the Department of Electrical Engineering, Colorado School of Mines, Golden, CO, USA in 2014. He joined the Erzurum Technical University in 2015 and served as an Assistant Professor until 2019. Since 2020, he has been serving as an Associate Professor with the Department of Electrical-Electronics Engineering, Sivas Cumhuriyet University, Turkey. His research interest includes numerical methods in electromagnetics, biological effect of electromagnetic radiation.



Atef Z. Elsherbeni received an honor B.Sc. degree in Electronics and Communications, an honor B.Sc. degree in Applied Physics, and a M.Eng. degree in Electrical Engineering, all from Cairo University, Cairo, Egypt, in 1976, 1979, and 1982, respectively, and a Ph.D. degree in Electrical Engineering from Manitoba University, Winnipeg, Manitoba, Canada, in 1987. He started his engineering career as a part time Software and System Design Engineer from March 1980 to December 1982 at the Automated Data System Center, Cairo, Egypt. From January to August 1987, he was a Post-Doctoral Fellow at Manitoba University. Elsherbeni joined the faculty at the University of Mississippi in August 1987 as an Assistant Professor of Electrical Engineering. He advanced to the rank of Associate Professor in July 1991, and to the rank of Professor in July 1997. He was the Associate Dean of the college of Engineering for Research and Graduate Programs from July 2009 to July 2013 at the University of Mississippi. He then joined the Electrical Engineering and Computer Science (EECS) Department at Colorado School of Mines in August 2013 as the Dobelman Distinguished Chair Professor. He was appointed the Interim Department Head for (EECS) from 2015 to 2016 and from 2016 to 2018 he was the Electrical Engineering Department head. In 2009 he was selected as Finland Distinguished Professor by the Academy of Finland and TEKES. Elsherbeni is a Fellow member of IEEE and ACES. He is the Editor-in-Chief for ACES Journal, and a past Associate Editor to the Radio Science Journal. He was the Chair of the Engineering and Physics Division of the Mississippi Academy of Science, the Chair of the Educational Activity Committee for IEEE Region 3 Section, the General Chair for the 2014 APS-URSI Symposium, the President of ACES Society from 2013 to 2015, and the IEEE Antennas and Propagation Society (APS) Distinguished Lecturer for 2020-2022.